



# Hydrophobic Interfacing of Fluorescent Membrane Probes

Felix Bayard,<sup>[a]</sup> Xiao-Xiao Chen,<sup>[a]</sup> Juan Manuel García-Arcos,<sup>[b]</sup> Aurelien Roux,<sup>[b]</sup> Naomi Sakai,<sup>[a]</sup> and Stefan Matile\*<sup>[a]</sup>

Fluorescent flippers have been introduced as small-molecule probes to image membrane tension in living systems. While the hydrophilic headgroup region has been modified extensively for intracellular targeting, little is known about the hydrophobic interfacing with the surrounding membrane. To tackle this challenge, the design, synthesis and evaluation of a glutamine-derived flipper collection is reported. Considering the importance of tension-induced phase separation for tension imaging, this study is focused on how to modulate the distribution of functional flippers between ordered and disordered micro-domains. Also of interest was control over intermembrane transfer without loss of function for the specific labeling of plasma and intracellular membranes. Evidence is presented for

a two-step insertion mechanism through more accessible disordered domains into better matching ordered domains. This process also explains differences between partition coefficients and bioimaging. It is further demonstrated that interdomain and intermembrane distribution can be regulated by hydrophobic interfacing to control brightness in fluorescence lifetime imaging microscopy and responsiveness to membrane tension. Irreversible partitioning inhibits intermembrane transfer and coincides with internalization into cells. These results demonstrate that hydrophobic interfacing can improve probe performance and provide guidelines on how to proceed.

## Introduction

Small-molecule fluorescent membrane probes are of central importance for bioimaging in living cells.<sup>[1–5]</sup> Depending on their design, the most common membrane probes respond to viscosity,<sup>[6–27]</sup> hydration,<sup>[1,3,26–40]</sup> thickness,<sup>[41–44]</sup> potential,<sup>[4,13–18,26,45–47]</sup> membrane order,<sup>[1–3,6,8,24,27–33]</sup> surface charge<sup>[39,40]</sup> and surface pH<sup>[12,36,48–50]</sup> by different mechanisms that mostly operate off equilibrium in the excited state. Fluorescent flippers have been introduced specifically as small-molecule probes to image membrane tension and order in living systems by mechanical compression in equilibrium in the ground state (Figure 1a–d).<sup>[5]</sup> For their design, the bioinspired<sup>[51,52]</sup> concept of planarizable push-pull probes has been formulated,<sup>[5,51]</sup> which remains different from other small-molecule approaches toward tension probes explored later on.<sup>[6–8,22,25,28,34,53]</sup> In brief, flipper probes are composed of two dithienothiophenes that are forced out of co-planarity by electrostatic repulsion from chalcogen-bond donors next to the twistable bond (Figure 1a, r). Mechanical planarization then

brings the two dithienothiophenes into conjugation, which induces bathochromic shifts of absorption and excitation maxima and increases in fluorescence lifetime and quantum yield. This red shift is enhanced significantly by non-covalent donors and covalent acceptors attached at both ends of the scaffold to turn-on a strong push-pull dipole in response to mechanical planarization (Figure 1a, r', a).

In aqueous media, the fully twisted flippers absorb in the blue, emit red shifted, and have a short fluorescence lifetime.<sup>[54]</sup> In lipid bilayers, flipper planarization with increasing order from liquid-disordered ( $L_d$ ) to liquid-ordered ( $L_o$ ) and solid-ordered ( $S_o$ ) membranes causes massive red shifts in excitation and equally distinct increases in fluorescence lifetime and intensity (Figure 1b). Membrane tension applied to single-component membranes ( $+\sigma$ ) decreases flipper lifetimes, which is consistent with probe deplanarization by mechanical lipid decompression (Figure 1c). In multi-component membranes, increasing lifetimes with tension indicate that the response is dominated by tension-induced membrane reorganization, particularly the formation of highly ordered microdomains with fully planarized flippers (Figure 1d).

With the objective to target any membrane of interest within cells, the hydrophilic head group of the original flipper 1 has been extensively varied.<sup>[5,50,55,56]</sup> In contrast, the hydrophobic tail region of flipper probes has remained largely unexplored.<sup>[57–59]</sup> This is because minimal changes in this region have mostly been detrimental for flipper function.<sup>[5]</sup> As a result, little is known about hydrophobic interfacing. There is much experimental and computational support that flipper probes align with the lipid tails of one leaflet of lipid bilayer membranes without disturbing their suprastructure significantly.<sup>[5,60,61]</sup> It is also known that Flipper-TR® 1 labels membranes of all orders, from  $L_d$  to  $S_o$  membranes. Moreover, the original Flipper-TR® 1 shows negligible flip-flop between

[a] F. Bayard, Dr. X.-X. Chen, Dr. N. Sakai, Prof. S. Matile  
Department of Organic Chemistry  
University of Geneva  
1211 Geneva (Switzerland)  
E-mail: stefan.matile@unige.ch

[b] Dr. J. M. García-Arcos, Prof. A. Roux  
Department of Biochemistry  
University of Geneva  
1211 Geneva (Switzerland)

Supporting information for this article is available on the WWW under  
<https://doi.org/10.1002/ceur.202300041>

© 2023 The Authors. ChemistryEurope published by Chemistry Europe and Wiley-VCH GmbH. This is an open access article under the terms of the Creative Commons Attribution License, which permits use, distribution and reproduction in any medium, provided the original work is properly cited.

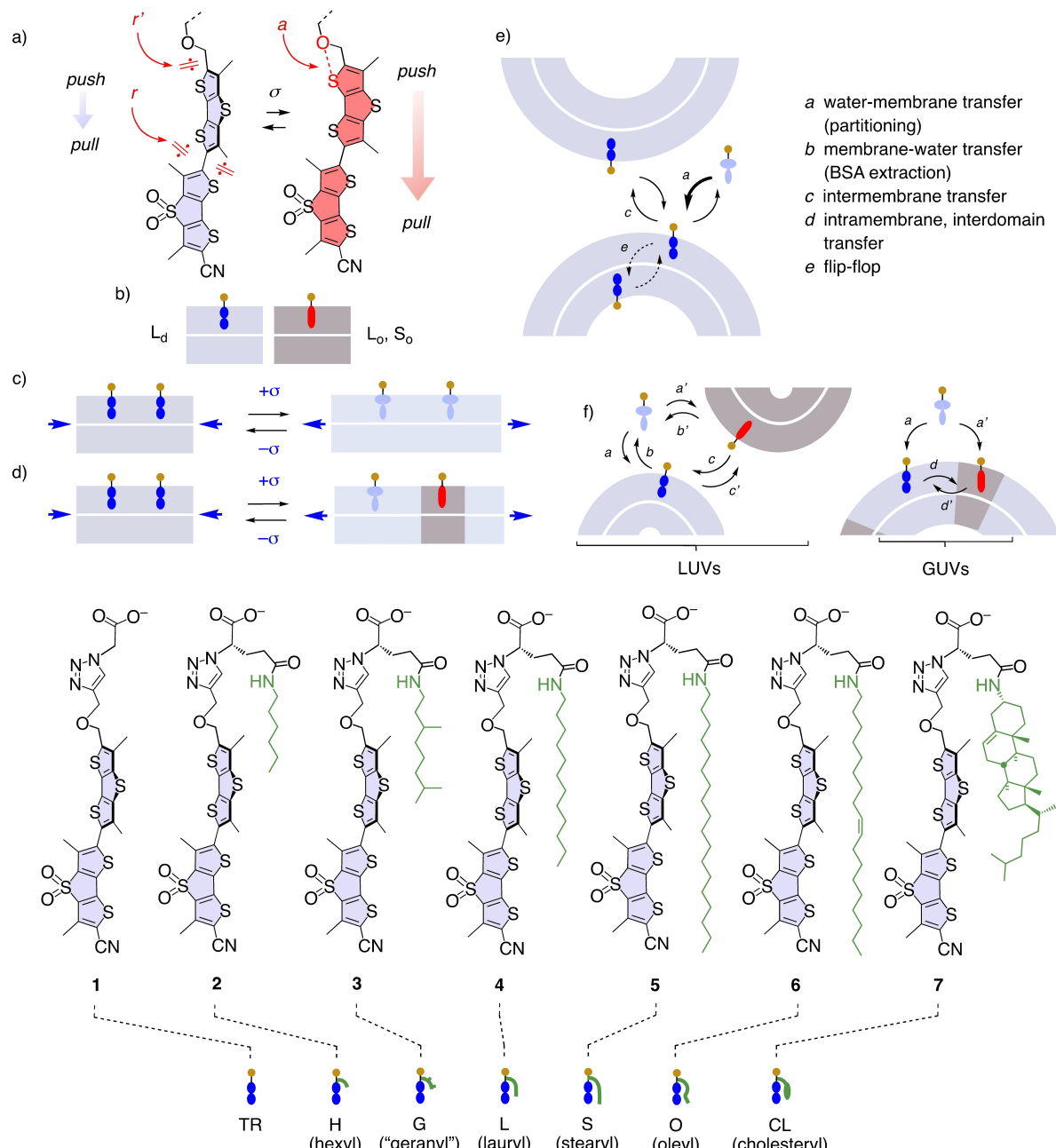


**Figure 1.** a) Planarization of flipper probes by mechanical forces  $\sigma$ , with indication of repulsive ( $r$ ) and attractive ( $a$ ) chalcogen bonding and push-pull dipoles. b) Planarization of flipper probes with increasing order, from liquid-disordered ( $L_d$ ) to liquid-ordered ( $L_o$ ) and solid-ordered ( $S_o$ ) membranes. c) In single-component membranes, flipper deplanarization with increasing tension indicates that probe response is dominated by membrane decompression. d) In multi-component membranes, flipper planarization with increasing tension indicates that probe response is dominated by membrane reorganization, particularly microdomain disassembly. e) Previously reported data demonstrate that Flipper-TR<sup>1</sup> rapidly jumps between different membranes (c) but fails to flip-flop between membrane leaflets (e). f) Processes explored in this study in LUVs and GUVs with flippers 1–7.

the two leaflets of the bilayer (Figure 1e, e)<sup>[62]</sup> but “jumps” freely through the media between the outer leaflets of different membranes (c).<sup>[63]</sup>

Considering that the contact with the surrounding membrane determines the response to membrane tension (Figure 1b–d),<sup>[5]</sup> a better understanding of hydrophobic interfacing is desirable. The term hydrophobic interfacing (or membrane interfacing) is used here to describe the topological matching between the hydrophobic part of the probe and the hydro-

phobic environment of the membrane, and structural modifications made to elaborate on this shape complementarity. Hydrophobic interfacing is a challenging topic of general concern for fluorescent membrane probes because they should disturb the supramolecular organization of their varying membrane environments as little as possible. Flipper probes should be particularly well suited to tackle this challenge because they sense small changes in the mechanics of their environment with high sensitivity. In this study, we report the design,



synthesis and evaluation of glutamine-derived flipper probes **2–7** to systematically explore hydrophobic interfacing in large LUVs and giant unilamellar vesicles (GUVs, Figure 1f). After an assessment of hydrophobic matching<sup>[38,44,64–67]</sup> of different interfacers with different membranes, the topics covered include control over water-to-membrane transfer (*a*), membrane-to-water transfer (*b*), intermembrane transfer (*c*) and intramembrane or interdomain transfer (*d*), in this order. For practical use (Figure 1d), we particularly wondered how to drive functional flippers into  $L_o$  and  $L_d$  domains (Figure 1f, *d*), suppress intermembrane transfer without loss of function (Figure 1f, *c*), and increase the various aspects of responsiveness by hydrophobic interfacing. The lessons learned will be helpful to design and also to characterize future flippers and fluorescent membrane probes in general.

## Results and Discussion

### Design and synthesis

The head group triad of the original Flipper-TR® **1** is composed of an ether, a triazole and a carboxylate (Figure 1).<sup>[5]</sup> The ether is essential as a non-covalent turn-on donor in the probes push-pull system for reasons that are not important for the topic of this study (Figure 1a, *r'*, *a*).<sup>[5,68]</sup> The triazole serves as a proton scavenger to prevent headgroup elimination.<sup>[5,69]</sup> The carboxylate assures plasma membrane labeling and suppresses background fluorescence by micelle formation in water.<sup>[5,70]</sup>

The headgroup triad is installed by a CuAAC click reaction with the respective alkynes and azides.<sup>[5,69]</sup> The amino acid glycine as the origin of the azide unit used to access the original Flipper-TR® **1** suggested that amino acids of free choice, natural and non-natural, should be clickable onto flipper probes. Glutamic acids carrying variable hydrophobic motifs attached to the side chain carboxylate were selected to elaborate on hydrophobic interfacing. The corresponding azido glutamines **8–13** were easily prepared and then clicked on the common flipper alkyne precursor **14** (Schemes 1, S1). Synthetic

access to flipper **14** in 14 steps has been reported and extensively optimized.<sup>[5]</sup>

The azidated glutamines **8–13** were obtained by reacting the doubly protected glutamate **15** with the respective alkyl amines **16–21**, followed by deprotection with acid and reaction of the resulting amines **22–27** with sulfonazide **28**. For reasonably varied interfacing, linear alkyl chains from a short C(6) hexyl (caproyl) in H-Flipper **2** to an intermediate C(12) lauryl in L-Flipper **4** and a long C(18) stearyl in S-Flipper **5** were complemented by a branched short C(10) tetrahydrogeranyl in G-Flipper **3** as a mixture of epimers, a long C(18) oleyl in O-Flipper **6** with a solubilizing *cis* double bond, and cholesteryl in CL-Flipper **7**.

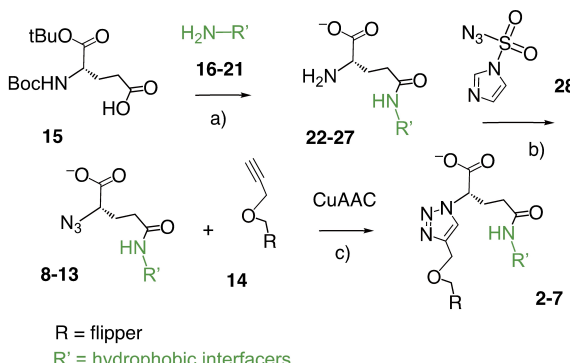
### Hydrophobic matching

Interfacing of the flipper collection **1–7** with lipid bilayers was explored first with regard to hydrophobic matching, that is the relation of interfacers length and membrane thickness. Alignment along the alkyl tails of one or both leaflets of a bilayer membrane has been shown to be best with matching length.<sup>[38,44,64–67]</sup> Weakly mismatched scaffolds are accepted but distort the membrane locally to swell or shrink. Strongly mismatched scaffolds either do not align and localize between the leaflets or at the surface, depending on their nature.

The importance of hydrophobically matched interfacing was probed in large unilamellar vesicles (LUVs) composed of C(18) distearoyl (DSPC), C(16) dipalmitoyl (DPPC) and C(14) dimyristoyl-sn-phosphatidylcholine (DMPC). The excitation spectra of all flippers except for the underperforming, mostly precipitating O-Flipper **6** and CL-Flipper **7** were recorded with decreasing temperatures (Figure 2a–c). Emission spectra were not very informative, as shown for the DPPC series (Figures 2d, S3, S4). This insensitivity of the emission is a characteristic of flippers compared to most other membrane probes, confirming that they operate by mechanical compression in equilibrium in the ground state.<sup>[5]</sup>

Measurements were started at 65 °C, where all membranes are in  $L_d$  phase. By stepwise cooling, a transition into the ordered phase was reported by the red shift of the excitation maximum. During cooling, the system was allowed to equilibrate at each recording temperature before the measurement was made. Confirming the importance of hydrophobic interfacing in general, the excitation spectra were not identical for all flippers, although they all contain the same mechanophore. These differences further confirmed that the mechanosensitivity of flipper probes is ideal to elaborate on hydrophobic interfacing, reporting small organizational changes in the environment with high sensitivity.

*Hydrophobic matching in thick membranes (DSPC, Figure 2a).* DSPC LUVs with long C(18) saturated tails at 65 °C are in the liquid-disordered  $L_a$  (aka  $L_d$ ) phase (Figure 2a).<sup>[71–73]</sup> Upon cooling, the phase transition into the phase-separated rippled  $P_{\beta'}$  phase occurs at 55 °C, followed by the transition into the solid-ordered  $L_{\beta'}$  (aka  $S_o$ ) at 49 °C, and then to the subgel  $L_c$  at 26 °C. Extensions of the disordered  $L_a$  phase down to 48.1 °C and



**Scheme 1.** Synthesis of flippers **2–7**; *R*, *R'* see Figure 1. a) 1. HBTU, DIPEA, DMF, rt, 0.5–1 h, 61–98%; 2. TFA,  $\text{CH}_2\text{Cl}_2$ , rt, 0.5–7 h, quant. b)  $\text{K}_2\text{CO}_3$ ,  $\text{CuSO}_4$  5  $\text{H}_2\text{O}$ , DMF, rt, 16 h, 20–81%. c) TBTA,  $\text{CuSO}_4$  5  $\text{H}_2\text{O}$ , sodium ascorbate,  $\text{CH}_2\text{Cl}_2$ /  $\text{H}_2\text{O}$  4:1, 1–4 h, rt, 34–89%.

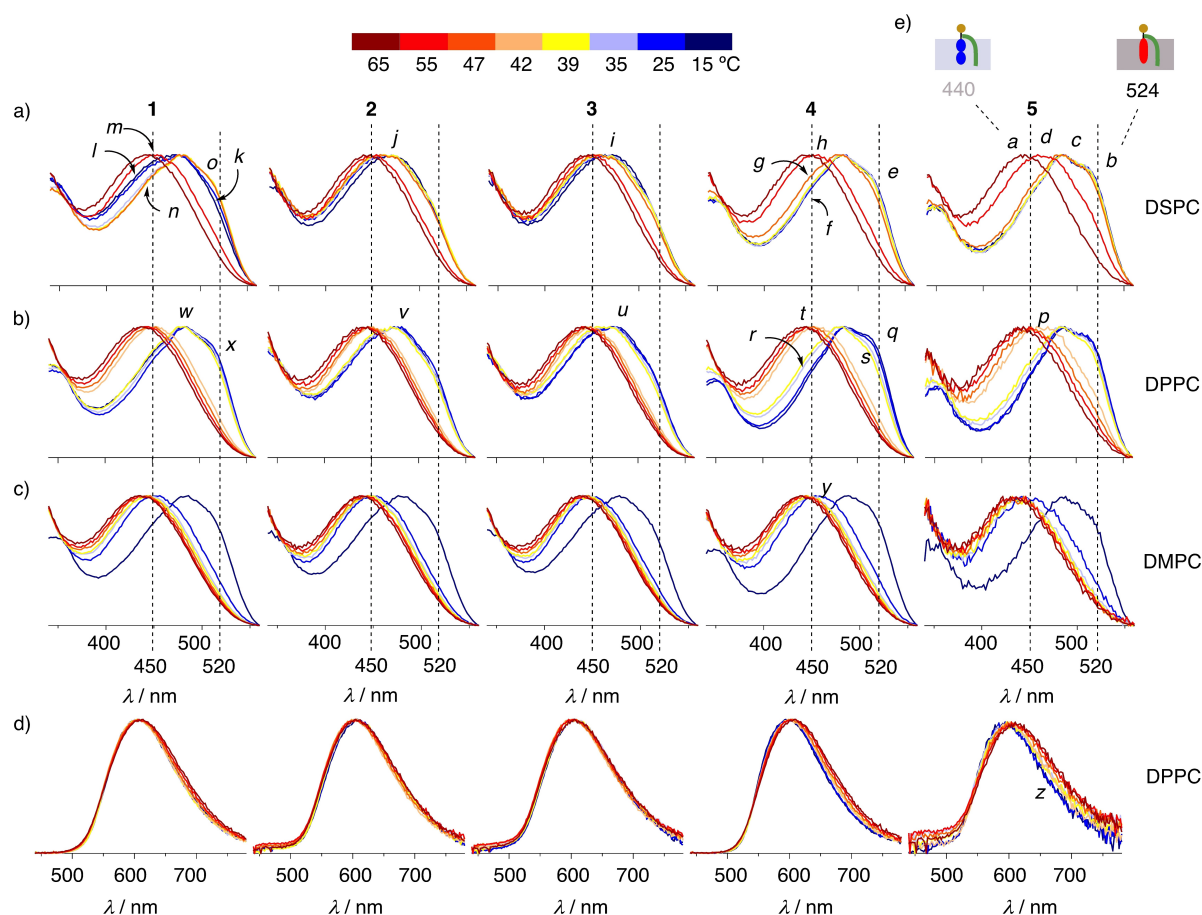


**Figure 2.** a-c) Excitation spectra of 1-5 (100 nM) in (a) DSPC, (b) DPPC and (c) DMPC LUVs with decreasing temperature from 65 °C to 15 °C; a-z direct discussion in the text. d) Emission spectra of 1-5 in DPPC with decreasing temperature from 65 °C to 15 °C. e) Schematic origin of blue and red shifted excitation from flipper deplanarization and planarization in disordered and ordered membranes, respectively.

rippled  $P_{\beta}$  phase down to 36.2 °C have been reported under special conditions, including SUVs and microdomains in multi-component membranes.<sup>[71-73]</sup>

**S-Flipper 5, DSPC LUVs.** Equipped with an interfacial length matching length, S-Flipper 5 reported the changes expected with DSPC LUVs with high precision and resolution. The blue-shifted excitation maximum at 444 nm at 65 °C (Figure 2a, a) was consistent with twisted flippers in the disordered  $L_a$  phase (Figure 1, 2e). The red-shifted maximum with vibrational finestructure below 47 °C (Figure 2a, b) was consistent with flipper planarization by mechanical compression from the surrounding solid-ordered  $L_{\beta}$  phase (Figure 1, 2e). Further transition to subgel  $L_c$  phase below 26 °C was not detected by S-Flipper 5. Spectral deconvolution placed the 0-0 transition at 524 nm (b) and the 0-1 transition at 492 nm (Figures 2a, c, 3b, Table S1). The intensity ratio of the 0-0 transition and the 0-1 transition in the deconvoluted spectrum was  $I_{0/1}=0.61$  (Figures 2a, b vs c, 3b). The following intensity ratio  $I_{1/2}$ , here  $I_{1/2} > 1$  (1.25), could be used as “positioning factor” to describe hydrophobic interfacing because the third band in deconvoluted spectra presumably contains also contributions from mispositioned, more twisted probes besides the 0-2 transition (Figure 3b). The excitation maximum of 5 at the phase transition in

DSPC LUVs was 458 nm, quite exactly in between the two extremes (Figure 2a, d).

**L-Flipper 4, DSPC LUVs.** Hydrophobic interfacing in DSPC LUVs with saturated alkyl chains was also possible with a slightly shorter length of the interfacial in L-Flipper 4. In the ordered  $L_c$  phase, the excitation spectrum was similar to that with S-Flipper 5, but overall slightly less red shifted because of a weaker 0-0 transition at unchanged 524 nm (Figures 2a, e, 3c). The vibrational ratio  $I_{0/1}=0.54$  was thus smaller, the positioning factor dropped to  $I_{1/2} \sim 1$  (i.e., 1.05). The third “positioning” transition became stronger at 47 °C, producing a distinct broadening on the left that coincided with a slightly smaller  $I_{0/1}=0.52$  at  $I_{1/2} < 1$  (i.e., 0.89, Figure S5), values that apparently report the transition of DSPC from rippled  $P_{\beta}$  to gel  $L_{\beta'}$  phase (g). At the  $P_{\beta}$  to  $L_a$  phase transition temperature at 55 °C, the excitation peak appeared more blue shifted at 458 nm and was poorly distinguishable from the disordered  $L_a$  phase at 65 °C with the maximum at 452 nm (h). The apparent preference by L-Flipper 4, but not S-Flipper 5, of the disordered to ordered phase DSPC suggested that matching length matters for hydrophobic interfacing, a qualitative interpretation that will receive further support in the following.

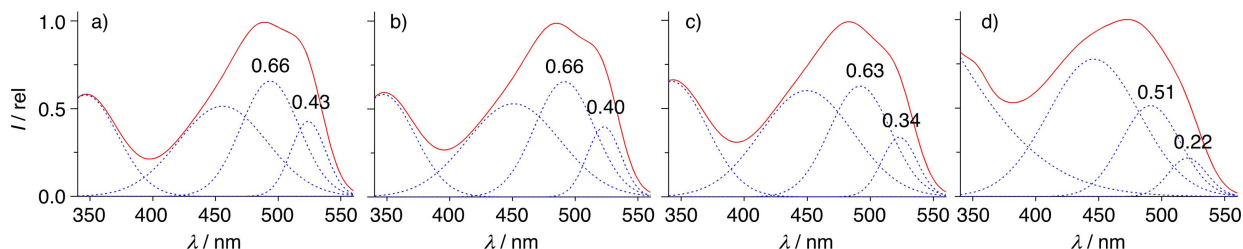


**Figure 3.** Deconvoluted excitation spectra of a) 4 in DPPC with  $I_{0/1}=0.65$ ,  $I_{1/2}>1$  (1.29), b) 5 in DPPC with  $I_{0/1}=0.61$ ,  $I_{1/2}>1$  (1.25), c) 4 in DSPC with  $I_{0/1}=0.54$ ,  $I_{1/2}\sim 1$  (1.05), and d) 1 in DSPC with  $I_{0/1}=0.43$ ,  $I_{1/2}<1$  (0.65), all at 15 °C, with indication of the relative intensity of the 0–0 transition at 524 nm and the 0–2 transition at 492 nm.

**Flippers 2–3, DSPC LUVs.** Poorer hydrophobic matching with the branched geranyl and short hexyl interfacers inhibited full planarization of G-Flipper 3 and H-Flipper 2 in DSPC LUVs. In  $L_{\beta'}$ -ordered phase, the excitation maximum blue shifted to 470 nm, and the vibrational finestructure disappeared (i, j; i.e.,  $I_{1/2}<1$ ).

**Flipper-TR 1, DSPC LUVs.** In clear contrast, the interfacers-free Flipper-TR® 1 showed red shifts and vibrational finestructure (k, l). However,  $I_{0/1}=0.43$  in  $L_c$  subgel phase was much smaller than with the better interfaced L-Flipper 4 as well as S-Flipper 5 (Figure 3d vs c, b). Together with a particularly intense 0–2-like shoulder at 446 nm (l, Figure 3d), this produced a broad and almost structureless peak with  $I_{1/2}<1$  (0.65) for Flipper-TR® 1 in  $L_c$  DSPC.

Flipper-TR® 1 poorly sensed the fluid to rippled phase transition at 55 °C like L-Flipper 4 (m). Upon transition from the rippled to gel  $P_{\beta'}-L_{\beta'}$  phase DSPC, the spectrum appeared red shifted compared to  $P_{\beta'}$  DSPC. This apparent red shift originated from a strong decrease of the 0–2 transition (n) and a weak increase of the 0–0 transition (o). Further cooling into subgel  $L_c$  phase caused the slight blue shift of the overall spectra. This behavior was unique, unlike with any other flipper in different membranes. It supported that whereas hydrophobic interfacing of Flipper-TR® 1 with solid-ordered  $L_{\beta'}$  DSPC is almost as good as with L-Flipper 4 and S-Flipper 5 ( $I_{1/2}\sim 1$ , i.e., 0.9 to 1.1, Figure S5, Table S1), that with subgel  $L_c$  DSPC is with  $I_{1/2}\ll 1$  suboptimal and can be improved significantly by hydrophobic interfacing, as demonstrated by L-Flipper 4 with  $I_{1/2}\sim 1$  and S-Flipper 5 with  $I_{1/2}>1$  (Figure 3b–d). The fingerprint of 1, 4, and 5 in DSPC LUVs was generally preserved at 4-fold dilution, confirming also that flipper probes in general act as monomers (Figure S2).<sup>[5]</sup>

**Hydrophobic matching in membranes of intermediate thickness (DPPC, Figure 2b).** Compared to DSPC, DPPC lipids have two carbons shorter C(16) saturated tails (Figure 2b). As a result, phase transition temperatures are lower. Cooling down from the liquid-disordered  $L_a$  phase, transitions occur at 41 °C to yield the rippled  $P_{\beta'}$ , at 34 °C to yield the solid-ordered  $L_{\beta'}$ , and at 19 °C to yield the subgel  $L_c$  phases.<sup>[71–73]</sup> Different rippled phases below and above 38.0 °C and a more ordered  $L_a$  preceding fully disordered  $L_a$  up to 48.7 °C have been reported under special conditions.<sup>[71–73]</sup>

**S-Flipper 5, DPPC LUVs.** The clean characteristics of S-Flipper 5 in DSPC LUVs were overall reproduced in DPPC LUVs, with the intermediate spectrum correctly appearing at 42 °C (Figure 2b, p

vs 2a, d). However, the spectra showed more noise, which reflected low fluorescence intensity, a result of probe precipitation dominating over partitioning. This change was consistent with poorer interfacing in DPPC compared to DSPC due to increased hydrophobic mismatch of the too long interfacers.

**L-Flipper 4, DPPC LUVs.** In clear contrast, the signature of L-Flipper 4 in DPPC LUVs was more impressive than in DSPC LUVs, nearly noiseless, testifying for preserved partitioning and improved interfacing due to better hydrophobic matching. Indeed, L-Flipper 4 in DPPC LUVs provided the best-structured spectra of the entire collection (Figure 2a–c, q–t). In ordered  $L_{\beta'}$  and  $L_c$  phase, the 0–0 transition at 524 nm was very strong (q), resulting in a record  $I_{0/1}=0.65$  with clear  $I_{1/2}>1$  (i.e., 1.3, Figures 2b, 3a). The rippled  $P_{\beta'}$  phase was perfectly reported at 39 °C and 35 °C with the characteristic broadening from a strong 0–2 transition at 448 nm (r) and a weak 0–0 transition at ~520 nm (s), resulting in lower  $I_{0/1}\sim 0.55$  and  $I_{1/2}\sim 1$  (i.e., 0.94 to 1.05, Figures 2b, S6). The maximum at the main phase transition temperature, 42 °C, was at 454 nm, cleanly placed in between the extremes. Above this temperature, gradual blue shifts were observed, implying an interesting gradual increase toward complete disorder at 446 nm (t).

**Flippers 2–3, DPPC LUVs.** G-Flipper 3 and H-Flipper 2 failed to reach full planarization also in solid-ordered DPPC. Improved interfacing with regard to interfacers length was however well reflected in the appearance of some vibrational finestructure in  $L_{\beta'}$  DPPC (u, v).

**Flipper-TR 1, DPPC LUVs.** The interfacers-free Flipper-TR® 1, almost dysfunctional in DSPC (Figure 2a, k–o), showed spectra with much stronger overall red shifts and vibrational finestructure in rippled  $P_{\beta'}$  and ordered  $L_{\beta'}$  DPPC (Figure 2b, w). Flipper-TR® 1, however, failed to differentiate between the two because the transition to ordered  $L_{\beta'}$  DPPC failed to further increase the 0–0 transition (x) and thus the comparably weak  $I_{0/1}=0.55$  with  $I_{1/2}\sim 1$  (i.e., 0.94 to 1.07, Figures 2b, S6). This was different from the best performing L-Flipper 4 with an excellent  $I_{0/1}=0.65$  and  $I_{1/2}>1$  (q vs x), indicating that also in DPPC, there is room for improvement by hydrophobic interfacing.

**Hydrophobic matching in thin membranes (DMPC, Figure 2c).** Shortening the tails again by two carbons down to C(14) in DMPC LUVs, phase transition temperatures further lowered to 24 °C for  $L_a$  to  $P_{\beta'}$  and 14 °C for  $P_{\beta'}$  to  $L_{\beta'}$  (Figure 2c).<sup>[71–73]</sup> Despite the accessibility to only  $P_{\beta'}$  but not  $L_{\beta'}$  even at 15 °C, all flippers produced strong red shifts with reasonable vibrational fines-



ture at this lowest measured temperature.  $L_a$  to  $P_{\beta'}$  phase transition around 25 °C (y, blue) and vibrational finestructure at higher order were again best visible with L-Flipper 4.<sup>[71–73]</sup>

In light of the lessons learned with excitation spectra, emission spectra were reconsidered (Figure 2d). While overall insensitivity toward membrane environments held and remained consistent with ultrafast planarization to and emission from a uniform PICT (planar intramolecular charge transfer)<sup>[74]</sup> state,<sup>[75,76]</sup> a small narrowing of the emission band from the most responsive L-Flipper 4 and particularly S-Flipper 5 (z) in  $L_c$ -DPPC was observed. This emission band narrowing coincided with the largest red shift, that is the strongest 0–0 transition in the excitation spectrum (p) and the largest positioning factor  $I_{1/2} > 1$ . These characteristics have been identified as indicative of maximal hydrophobic interfacing. Such maximal hydrophobic interfacing should coincide with minimal hydration around the planarized push-pull probe. Minimal hydration, in turn, should minimize solvatochromism.<sup>[1,54]</sup> The small blue shift of the emission thus supported that maximized hydrophobic interfacing also minimizes hydration around the probe, which is reflected by a small blue shift of the emission maximum.<sup>[54]</sup> Compared to the impact of mechanical compression in equilibrium in the ground state on the excitation spectra (Figure 2a, b), the impact of membrane dehydration on solvatochromism in the emission spectra is minor and without importance for use in practice (Figure 2d).

Taken together, comprehensive analysis with the flipper collection 1–5 in DSPC, DPPC and DMPC LUVs revealed that the original, interfacser-free Flipper-TR® 1 reports membrane order best in DPPC but less convincingly in DSPC, and that hydrophobic interfacing can improve flipper performance in all membranes with regard to apparent red shifts, vibrational finestructure, positioning factor in deconvoluted spectra, and responsiveness toward phase transition and subphases. The overall best-performing probe in LUVs is L-Flipper 4 with a C(12) lauryl interfacser, most impressive in DPPC LUVs. In general, different excitation fingerprints for identical mechano-phores confirm that hydrophobic interfacing is significant for probe performance and deserves attention. With hydrophobic interfacing being far from perfect, this conclusion implies that further improvements in flipper performance by hydrophobic matching should be possible.

### Addition to membranes

LogP's, the partition coefficients between octanol, a "bulk membrane", and water, were computed for the sodium salts of flippers 1–7 (Figure 4a). Four different methods gave identical trends, and average values are reported (XLOG3, WLOGP, SILICOS-IT (SwissADME),<sup>[77]</sup> CLOGP (ChemDraw)). The computed LogP values increased gradually with size of the hydrophobic interfacser. The calculated solubility in water decreased gradually from 16 nM for 1 to 460 pM for 2, 23 pM for 3, 3.4 pM for 4, 0.024 pM for 5, 0.084 pM for 6 and 0.7 fM for 7. At concentrations above these values in water, flipper amphiphiles are

expected to self-assemble into micelles<sup>[5,70]</sup> and ultimately precipitate.

Partition coefficients  $K_x$  quantify the transfer from water to lipid bilayer membranes (Figure 1f, a, a'). They were determined following standard procedures at 37.5 °C.<sup>[57,78]</sup> Changes in fluorescence intensity were measured for increasing lipid concentration at constant flipper concentration (Figure S8). Data analysis revealed that the original Flipper-TR® 1 partitions preferably into  $L_d$  DOPC membranes (Figures 4b, 1f, a, Table S2). With increasingly hydrophobic but mismatched interfacers in H-Flipper 2 and G-Flipper 3, partitioning into  $L_d$  membranes further increased. Beginning with L-Flipper 4, partitioning into  $L_d$  LUVs dropped sharply with further increasing hydrophobicity (Figure 4b). This decrease was contrary to expectations from LogP (Figure 4a). It implied that at LogP > 17 with a solubility in water < 20 pM, flippers failed to reach the membrane, assembled into ultrastable, non-emissive micelles and ultimately precipitated.

In biology,  $L_o$  membranes are more important than  $S_o$  membranes.  $L_o$  membranes are formed by saturated lipids and cholesterol. Within a distinct area in the three-component phase diagrams, they phase separate from the  $L_d$  membranes of unsaturated lipids.<sup>[79,80]</sup> Partition coefficients  $K_{xo}$  for  $L_o$  membranes were measured in LUVs composed of sphingomyelin (SM) and cholesterol (CL) in the ratio of 7:3. H-Flipper 2 partitioned best into SM/CL 7:3 membranes (Figures 4c, 1f, a', Table S2). With increasing interfacser length, partition coefficients decreased, in part because of decreasing solubility. With the more hydrophobic interfacers, results were of limited significance because competing precipitation lowered fluorescence intensity toward the limit of meaningful detectability.

As this solubility problem already affected partitioning into  $L_d$  membranes (Figure 4b), the fractional  $K_{o/d}$ , dividing  $K_{xo}$  with  $L_o$  by  $K_{xd}$  with  $L_d$  membranes, should nevertheless yield a rather meaningful approximation for the discrimination of flipper probes between membranes of different order (Figure 4d, Table S1). According to  $K_{o/d} = 0.07$ , the original Flipper-TR® 1 showed a strong, ~15 fold selectivity for  $L_d$  membranes. Similarly strong preference of G-Flipper 3 was consistent with a poor fit of branched interfacers with ordered membranes. H-Flipper 2 and L-Flipper 4 with shorter hydrophobic interfacers reduced this  $L_d$  preference but failed to invert selectivity.

The inversion of selectivity from  $L_d$  to  $L_o$  was achieved with the S-Flipper 5 of matching length and shape. The obtained record  $K_{o/d} = 2.7$  was, however, of little importance because dominant probe precipitation lowered fluorescence intensity below significance for practical use in bioimaging. Solubilization with a *cis* double bond at the constant length of the interfacser in O-Flipper 6 improved fluorescence intensity at the cost of  $L_o$  selectivity, confirming that matching shape is more important than matching length for hydrophobic interfacing. While self-sorting among *cis* unsaturated flippers and  $L_d$  membranes against saturated flippers and  $L_o$  membranes was thus operational to a certain extent, cholestryl interfacers failed to drive CL-Flipper 7 into the CL-rich  $L_o$  membranes. The non-selective

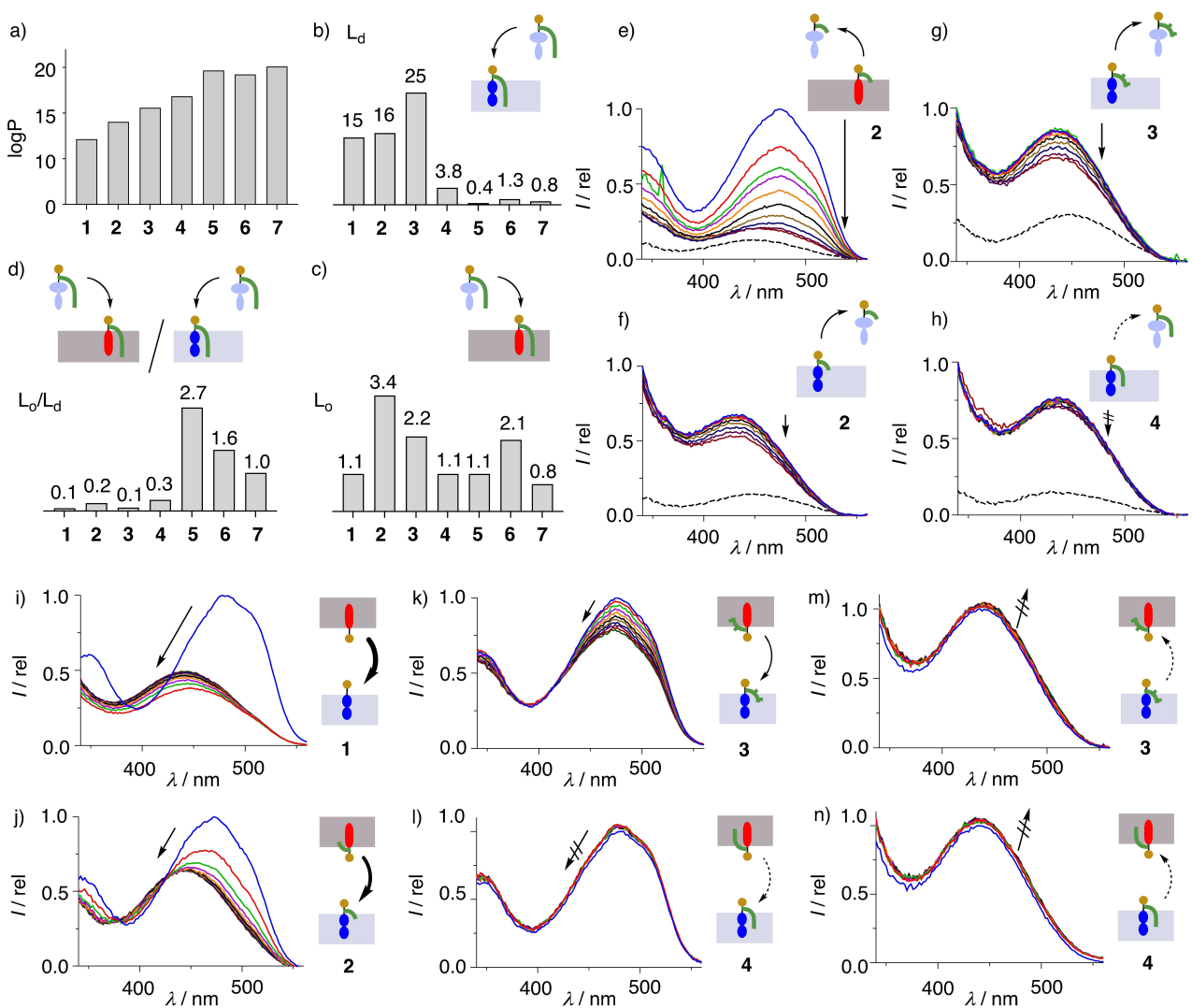


**Figure 4.** Addition to membranes (a–d), extraction from membranes (e–h), and intermembrane transfer (i–n). a) Computed octanol/water partition coefficients (sodium salts). b)  $K_{xd} = K_x$  for 1–7 in  $L_d$  DOPC membranes ( $\times 10^6$ ). c)  $K_{xo} = K_x$  for 1–7 in  $L_o$  SM/CL 7:3 membranes ( $\times 10^6$ ). d)  $K_{o/d} = K_{xo}/K_{xd}$  for 1–7. e–h) Excitation spectra of e) 2 in SM/CL 7:3 and f) 2, g) 3 and h) 4 in DOPC LUVs with increasing concentrations of BSA (0–40  $\mu$ M, dashed lines: flippers with BSA (40  $\mu$ M) without LUVs). i–l) Excitation spectra of i) 1, j) 2, k) 3 and l) 4 in SM/CL LUVs with time after addition of DOPC LUVs (0–5 min). m–n) Excitation spectra of flippers m) G 3 and n) L 4 in DOPC LUVs with time after addition of SM/CL LUVs (0–5 min).

$K_{o/d} = 1.0$  of CL-Flipper 7 should, however, not be overinterpreted because of the above-mentioned solubility issues.

### Extraction from membranes

The reversibility of water to membrane transfer (Figure 1f, a, a') described by the partition coefficients (Figure 4a-d) was determined by extracting flippers from membranes with bovine serum albumin (BSA, Figures 1f, b, b', 4e–h). Binding of flippers to BSA produced a very weak excitation maximum around 450 nm, suggesting that they are not much planarized by the protein (Figure 4e–h, dashed spectra).<sup>[63]</sup> Extraction of planarized flippers from  $L_o$  LUVs by adding BSA was thus detectable by partial deplanarization, that is a small blue shift and a strong decrease in intensity (Figure 4e). BSA extraction of more twisted flippers from  $L_d$  membranes occurred with a small red shift but

still decreasing intensity (Figure 4f–h). The effective concentration of BSA to extract Flipper-TR® 1 from  $L_o$  membranes has been determined previously at  $EC_{50} = 0.7 \mu\text{M}$ .<sup>[63]</sup>

H-Flipper 2 could be extracted with BSA from  $L_o$  and  $L_d$  membranes at about the same  $EC_{50}$  (Figure 4e,f). The same was true for G-Flipper 3 (Figures 4g, S9). BSA, however, failed to extract L-Flipper 4 from  $L_o$  and  $L_d$  membranes (Figure 4h). BSA extraction of flippers 5–7 with more hydrophobic interfacers was not detectable either, but their poor solubility hindered the acquisition of high quality data as described above (Figure S9). Extractability of the similarly bulky G-Flipper 3 suggested that binding of L-Flipper 4 to BSA should be preserved sufficiently. The failure to extract 4 from membranes should thus originate from maximized interfacing.



## Intermembrane transfer

The combination of extraction from membranes and addition to membranes adds up to intermembrane transfer. Intermembrane transfer stands for the movement of probes through the media from the outer leaflet of one membrane to the outer leaflet of another membrane (Figure 1e, c). This “membrane hopping” through space is important in bioimaging. Photo-cleavable flipper probes for targeted release, for instance, have been directed to the outer membrane of the ER.<sup>[63]</sup> Upon release with light, they instantaneously transferred through space to all accessible membranes facing the cytosol and stained the inner leaflet of the plasma membrane selectively because the highest order produces the strongest emission from planarized probes (Figure 1e, c). Released in the inner leaflet of ER membranes, flipper probes, incapable of flip-flop (Figure 1e, e), stained the ER and migrated with time along the secretory pathway to the Golgi and the outer leaflet of the plasma membrane.<sup>[62]</sup> Control over intermembrane transfer would thus be essential for targeted release in membranes of interest within cells.

To explore the impact of hydrophobic interfacing on intermembrane transfer, flipper probes were first added to  $L_o$  SM/CL LUVs. Then,  $L_d$  DOPC LUVs were added, and the changes in the excitation spectra were recorded with time. For the interfacial-free Flipper-TR® 1, the fluorescent signature of planarized flippers in  $L_o$  SM/CL LUVs disappeared within  $t_{1/2}=1.8$  seconds and was replaced by that of twisted flippers in  $L_d$  DOPC LUVs (Figure 4i).<sup>[63]</sup> Intermembrane transfer decelerated with increasing hydrophobic matching from H-Flipper 2 with  $t_{1/2}=17$  seconds (Figure 4j) to G-Flipper 3 with incomplete transfer within 5 min (Figure 4k). Within the same timeframe of 5 min, intermembrane transfer of L-Flipper 4 was not detectable (Figure 4l). Significant reverse transfer from  $L_d$  DOPC LUVs to  $L_o$  SM/CL LUVs was detectable neither for G-Flipper 3 (Figure 4m) nor from L-Flipper 4 (Figure 4n). These trends for intermem-

brane transfer (Figures 4i–n, S10) were exactly as for the extraction from membranes with BSA (Figures 4e–h, S9). They confirmed that increasing hydrophobic interfacing can inhibit intermembrane transfer.

## Intramembrane transfer

Intramembrane transfer of fluorescent probes by lateral diffusion describes the distribution between different domains within the same membrane leaflet.<sup>[2]</sup> Control over interdomain distribution was of interest with flipper probes because the imaging of membrane tension in living cells reports on changes in membrane organization, particularly tension-induced microdomain dis/assembly (Figure 1d). Moreover, it was of interest to compare fractional partition coefficients  $K_{o/d}$  determined in single-component membranes (Figure 4d) and probe distribution in phase-separated multi-component membranes.

Intramembrane transfer was assessed by fluorescence lifetime imaging microscopy (FLIM) of GUVs composed of single-component  $L_d$  and  $L_o$  membranes and multi-component membranes that contain  $L_d$  and  $L_o$  domains.<sup>[79,80]</sup> As far as possible, the longer lifetimes  $\tau_1$  after biexponential fit were recorded for all flippers 1–7 in all GUVs (Figure 5). Lifetimes of flippers 1–7 in single-component  $L_d$  DOPC GUVs were similar to each other, reaching from  $\tau_1=3.4$  ns (1) to  $\tau_1=3.6$  ns (7, Table S3, Figures 5a, S12). Also similar were the lifetimes in single-component  $L_o$  SM/CL GUVs, if reliably detectable, from  $\tau_1=5.3$  ns (4) to  $\tau_1=6.0$  ns (1, Table S3, Figures 5b, S12). Increasing lifetime with increasing membrane order was consistent with increasing flipper planarization in the ground state, as observed and discussed previously (Figure 1b).<sup>[5]</sup> For the direct detection of intramembrane transfer, FLIM images of phase-separated multi-component GUVs composed of DOPC/SM/CL 58:25:17 were essential.

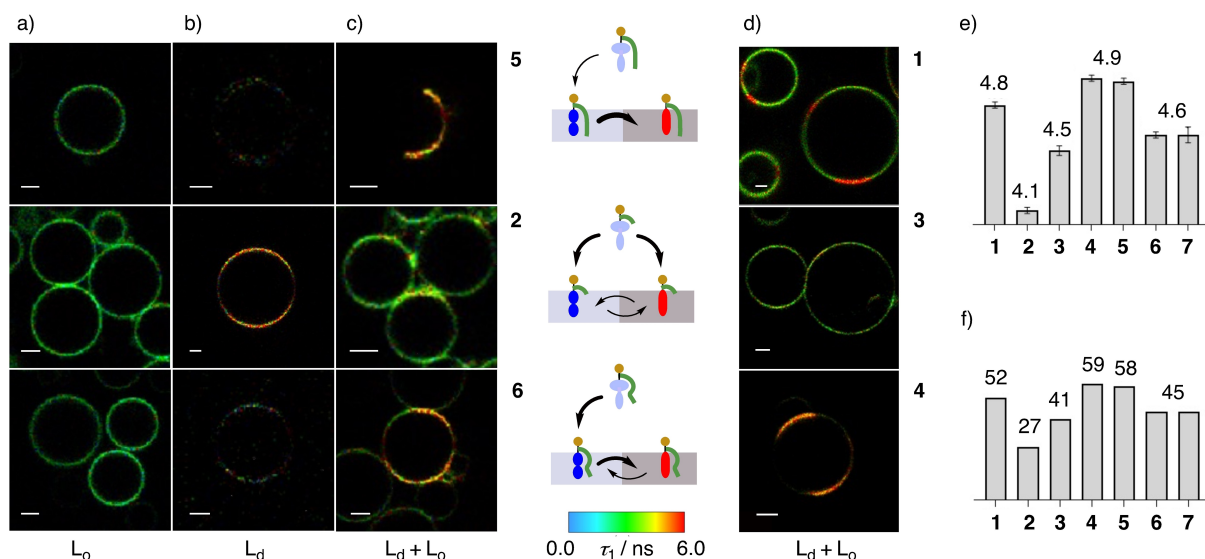


**Figure 5.** a–c) FLIM images of 5 (top), 2 (middle) and 6 (bottom) in GUVs composed of a) DOPC, b) SM/CL 7:3 and c) DOPC/SM/CL 58:25:17. d) FLIM images of 1 (top), 3 (middle) and 4 (bottom) in DOPC/SM/CL 58:25:17 GUVs, with e) global fluorescence lifetimes  $\tau_1$  in DOPC/SM/CL 58:25:17 GUVs, f) calibrated against  $\tau_1$  of 1 in SM/CL (6.0 ns, 100%) and in DOPC GUVs (3.4 ns, 0%) to estimate selectivity for  $L_o$  domains in %, scale bars = 3  $\mu$ m.



**Flipper-TR 1.** Confirming previous reports,<sup>[59]</sup> the original Flipper-TR® 1 emitted from both domains of DOPC/SM/CL GUVs (Figures 5d). FLIM intensity, corresponding to the number of counts in the FLIM images, was higher from L<sub>o</sub> domains (Table 1). The overall lifetime  $\tau_{o+d}=4.8$  ns in phase-separated multi-component GUVs was in between the isolate lifetimes  $\tau_o$  in single-component L<sub>o</sub> (6.0 ns) and  $\tau_d$  in single-component L<sub>d</sub> membranes (3.4 ns, Figure 5e, Table S3). Calibrated against the isolate lifetimes  $\tau_o$  and  $\tau_d$  in multi-component GUVs,  $\tau_{o/d}=(\tau_{o+d}-\tau_d)/(\tau_o-\tau_d)\times 100\%$  was calculated to estimate intra-membrane transfer. The obtained  $\tau_{o/d}=52\%$  seemingly implied that about half of Flipper-TR® 1 partitioned into L<sub>o</sub> domains (Figure 5f, Table 1). This equal distribution according to lifetime analysis in multi-component L<sub>o</sub>+L<sub>d</sub> GUVs was in disagreement with the 15-fold preference for L<sub>d</sub> over L<sub>o</sub> LUVs determined from fractional partition coefficients  $K_{o/d}$  (Figure 4d, Table 1).

**H-Flipper 2.** These apparently contradictory trends with Flipper-TR® 1 were present but less pronounced with H-Flipper 2 (Figure 5a–c, middle). FLIM in single-component L<sub>d</sub> GUVs revealed homogeneous labeling with  $\tau_1=3.4$  ns and without anisotropy (Figure 5a, middle, Table S3). In single-component L<sub>o</sub> GUVs, FLIM images showed much higher  $\tau_1=5.5$  ns, as expected from flipper planarization by physical compression from the more ordered environment (Figure 5b, middle, Table S3). The emergence of dark equator regions, indicating strong anisotropy, was consistent with a firmer flipper alignment along the more ordered lipid tails. In DOPC/SM/CL 58:25:17 GUVs, L<sub>d</sub> domains were labeled stronger L<sub>o</sub> domains (Figure 5c, middle). The overall lifetime  $\tau_{o+d}=4.1$  ns in phase-separated multi-component GUVs (Figure 5e) calculated to only 27% of H-Flipper 2 localizing in L<sub>o</sub> domains (Figure 5f). This preference for L<sub>d</sub> membranes of the mismatched H-Flipper 2

was reasonably consistent with  $K_{o/d}=0.2$  (Figure 4d) and a low positioning factor  $I_{1/2} < 1$  in single-component LUVs (Figures 2, 3), and comparably strong FLIM intensity in L<sub>d</sub> domains in multi-component phase-separated GUVs (Figure 5c, Table 1).

**S-Flipper 5.** Direct experimental evidence for the existence of an almost exclusive two-step partitioning into matching L<sub>o</sub> domains through more accessible L<sub>d</sub> domains could be obtained with S-Flipper 5 (Figure 5a–c, top). While probe addition to L<sub>d</sub> membranes gave the usual uniform labeling (Figure 5a, top), addition to L<sub>o</sub> membranes did not afford any labeled GUVs (Figure 5b, top). However, added to DOPC/SM/CL 58:25:17 GUVs, S-Flipper 5 selectively labeled the L<sub>o</sub> domains (Figure 5c, top). Without evidence from long lifetimes and high anisotropy, this inversion of selectivity from L<sub>d</sub> to L<sub>o</sub> membranes could not be detected, and results would be misinterpreted. However, with the information provided by the mechanosensitive flipper probe, the inversion of selectivity from L<sub>d</sub> to L<sub>o</sub> in biomimetic multi-component membranes revealed the occurrence of two-step partitioning through the better accessible L<sub>d</sub> into the better matching L<sub>o</sub> domains. The overall lifetime  $\tau_{o+d}=4.9$  ns suggested that 58% of S-Flipper 5 partitioned into L<sub>o</sub> domains (Figure 5e, f). This consistent preference for L<sub>o</sub> membranes of S-Flipper 5 was well reflected in  $K_{o/d}=2.7$  (Figure 4d) and  $I_{1/2} > 1$  in LUVs (Figures 2, 3). However, neither data from LUVs nor  $\tau_{o/d}=58\%$  ns would predict the specificity for L<sub>o</sub> labeling found in FLIM images (Figure 5c, Table 1).

**O-Flipper 6.** In O-Flipper 6, the solubilizing central *cis* double bond at preserved length compared to the saturated S-Flipper 5 was impactful (Figure 5a–c, bottom). Single-component L<sub>o</sub> membranes became very weakly detectable in FLIM images of GUVs (Figure 5b, bottom). More importantly, L<sub>d</sub> domains became clearly detectable in multi-component membranes (Figure 5c, bottom). These differences were significant enough to reduce total lifetimes to  $\tau_{o+d}=4.6$  ns and partitioning into L<sub>o</sub> domains to 45% (Figures 5e,f). This result confirmed that also at matching length, matching shape is significant for hydrophobic interfacing. Despite overall correct trends, the formal inversion from weak L<sub>o</sub> to weak L<sub>d</sub> selectivity with a central *cis* double bond (Figure 5f) was not predicted by fractional partition coefficient  $K_{o/d}=1.6$  in LUVs (Figure 4d, Table 1). The same  $\tau_{o+d}=4.6$  ns was noted also for CL-Flipper 7, although very low intensities due to dominant precipitation made these data less reliable (Figure 5e).

**Flippers 3 and 4.** Topological mismatch of G-Flipper 3 with regard to both interfacial length and shape provided access to the bright L<sub>d</sub> labeling in FLIMed GUVs (Figure 5d, middle). However, global lifetime  $\tau_{o+d}=4.5$  ns remained above H-Flipper 2, and L<sub>d</sub> selectivity dropped correspondingly from 73% to 59% (Figures 5e,f). In clear contrast, L-Flipper 4, best performing in LUVs (Figure 2), gave bright FLIM images with dominant labeling of L<sub>o</sub> domains (Figure 5d, bottom). L<sub>d</sub> domains remained slightly visible, which resulted in record  $\tau_{o+d}=4.9$  ns and thus 59% selectivity for L<sub>o</sub> domains (Figure 5f). Almost specific L<sub>o</sub> labeling in GUVs would not have been predicted from  $K_{o/d}=0.3$  in LUVs, while as for 5,  $I_{1/2} > 1$  predicted specific L<sub>o</sub> labeling in GUVs best (Table 1).

**Table 1.** Comparison of data from GUVs ( $I_{Lo}$ ,  $I_{Ld}$ ,  $\tau_{o/d}$ ), LUVs ( $K_{o/d}$ ,  $I_{1/2}$ ) and cells ( $\tau_i$ ,  $\tau_h$ ).<sup>[a]</sup>

F <sup>[b]</sup>	$I_{Lo}$ <sup>[c]</sup>	$I_{Ld}$ <sup>[d]</sup>	$\tau_{o/d}\%[e]$	$K_{o/d}$ <sup>[f]</sup>	$I_{1/2}$ <sup>[g]</sup>	$\tau_i/\tau_h$ /ns <sup>[h]</sup>
1	++	++	52	0.1	0.65	5.5/5.0
2	++	+++	27	0.2	0.91	5.1/(4.5)
3	++	++	41	0.1	0.78	5.2/(4.5)
4	++	+	59	0.3	1.05	5.3/(nd)
5	++	-	58	2.7	1.25	5.2/(nd)
6	++	++	45	1.6	nd	5.3/(nd)
7	nd	nd	45	1.0	nd	(nd)

[a] nd = not detected. [b] Flipper (Figure 1). [c] Intensity of (lifetime counts for) L<sub>o</sub> domains in FLIM images of L<sub>o</sub>+L<sub>d</sub> GUVs. [d] Intensity of L<sub>d</sub> domains in FLIM images of L<sub>o</sub>+L<sub>d</sub> GUVs. [e] Percentage of probes in L<sub>o</sub> domains in L<sub>o</sub>+L<sub>d</sub> GUVs from normalized lifetimes  $\tau_{o+d}$  in FLIM images of multi-component L<sub>o</sub>+L<sub>d</sub> GUVs:  $\tau_{o/d}=(\tau_{o+d}-\tau_d)/(\tau_o-\tau_d)\times 100\%$ . Here,  $\tau_o$  and  $\tau_d$  of 1 were used for all flippers (6.0 and 3.4 ns, respectively). [f] Fractional partition coefficient in single-component LUVs ( $K_{o/d}=K_{xo}/K_{xd}$ ). [g] Positioning factor from deconvoluted excitation spectra in DSPC LUVs at 15 °C (Table S1). [h] Lifetimes  $\tau_1$  of flippers in plasma membranes in FLIM images of HK cells under isoosmotic (i) and hyperosmotic (h) conditions (plasma membrane values in parenthesis measured selectively excluding internalized probes).



Taken together, the visual impression of selective  $L_o$  labeling in FLIM images of multi-component GUVs in the order  $5 > 4 > 1 \sim 6 > 2 \sim 3$  was in agreement with expectations from interfacial structure (Table 1). Mean FLIM lifetimes in multi-component GUVs ( $4 \sim 5 > 1 > 6 > 3 > 2$ ) and positioning factors in single-component LUVs ( $5 > 4 > 2 > 3 > 1$ ) reproduced the selectivity sequence reasonably well, including meaningful outliers. In clear contrast, partition coefficients from single-component LUVs were non-predictive ( $5 > 6 \gg 4 > 2 > 3 \sim 1$ ). The general underestimation of  $L_o$  labeling from partitioning data in single-component LUVs originates from the higher fluorescence intensity of planarized flippers in  $L_o$  compared to twisted flippers in  $L_d$  domains of multi-component phase-separated GUVs, which increases the respective counts in  $L_o$  domains in FLIM images. The larger offset of partitioning data from single-component membranes in LUVs originates from two-step partitioning in multi-component membranes, first from water into the more accessible  $L_d$  domains and from there into the better matching  $L_o$  domains. The existence of this process is best illustrated with S-Flipper 5 in GUVs (Figure 5a–c, top).

From the available single-component LUV data, the new positioning factors from vibrational finestructure  $I_{1/2}$  in  $L_o$  LUVs predicted matching interfacing for  $L_o$  labeling overall best. For direct spectroscopic prediction of two-step partitioning with LUVs, Flipper-TR® 1 was added first to a 1:1 mixture of  $L_o$  LUVs (SM/CL 7:3) and  $L_d$  LUVs (DOPC). The obtained excitation spectrum matched the one in  $L_d$  LUVs (DOPC), indicating the selective partitioning of Flipper-TR® 1 into  $L_d$  membranes, as predicted from partition coefficients  $K_{o/d} = 0.1$  (Figure 6a, blue). Then Flipper-TR® 1 was added to phase-separated multi-component LUVs containing 42% (green) and 70% (red)  $L_o$  domains (DOPC/SM/CL). With increasing  $L_o$  domains, the excitation spectrum shifted to the red. At 70%  $L_o$  domains, the spectrum resembled the one in single-component  $L_o$  LUVs with visible 0–0 transition.

Similar overall trends were observed for H-Flipper 2 in the same set of experiments (Figure 6b). However, at 70%  $L_o$  domains, the spectrum of 2 was less red shifted and finestructured. This difference confirmed the impression from FLIM images in GUVs that the H-Flipper 2 labels  $L_d$  domains better than Flipper-TR® 1 and does less diffuse into the mismatched  $L_o$  domains (Figure 6, Table 1, entry 1, 2).

These spectra were deconvoluted to estimate the fractions of flipper probes in  $L_o$  (red) and  $L_d$  (green) membranes assuming the spectra to be the mathematical sum of those in single-component membranes (Figure 6c–e). Quantification with correction for the high and low intensities in  $L_o$  and  $L_d$  membranes, respectively, gave 51% 1 and 40% 2 in  $L_o$  domains of multi-component LUVs. This was in reasonable agreement with 52% 1 and 27% 2 in  $L_o$  domains of multi-component GUVs obtained from FLIM lifetimes (Figure 5f).

### Cellular Response

The impact of hydrophobic interfacing on bioimaging was assessed in HeLa Kyoto (HK) cells under routine conditions.

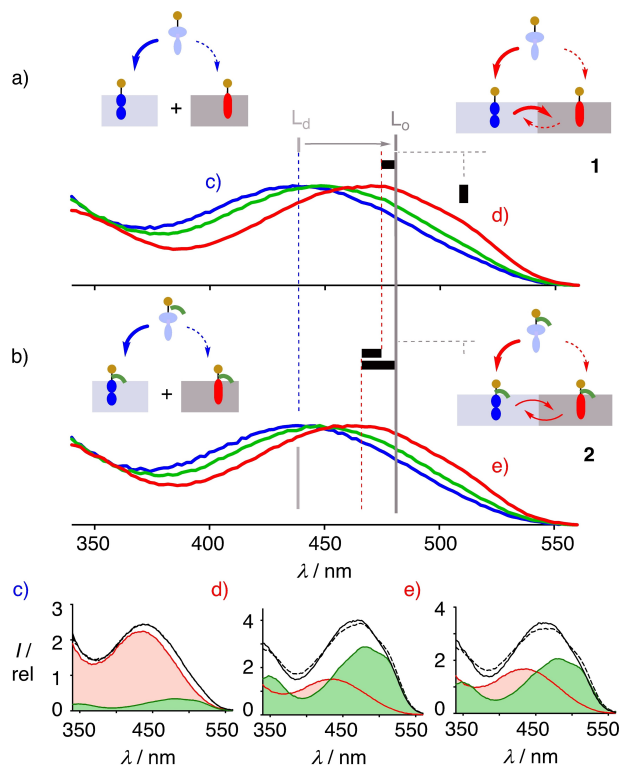


**Figure 6.** Excitation spectra of a) 1 and b) 2 in a 1:1 mixture of DOPC and SM/CL LUVs (50%  $L_o$  isolate, blue) and phase-separated multi-component LUVs, formally containing 42%  $L_o$  (DOPC/SM/CL 58:25:17, green) and 70%  $L_o$  domains (DOPC/SM/CL 3:4:3, red). c–e) Deconvolution of spectra for c) 1 in a 1:1 mixture of  $L_o$  and  $L_d$  LUVs (blue in a) and d) 1 (red in a) and e) 2 (red in b) in multi-component membranes into spectra of 1 and 2 in  $L_d$  (red) and  $L_o$  LUVs (green).

Added to HK cells, Flipper-TR® 1 selectively labeled the plasma membrane as reported (Figure 7a).<sup>[5]</sup> In response to hyperosmotic stress, the lifetime in FLIM images decreased (Figure 7b), which is consistent with flipper deplanarization, thus reporting on membrane reorganization, particularly microdomain disassembly, upon reduction of membrane tension (Figure 1d).

H-Flipper 2 and G-Flipper 3 labeled the plasma membrane similarly well (Figure 7a). After the osmotic shock, both showed significant internalization, labeling internal membranes of reduced order (Figure 7b). The more hydrophobic flippers 4–7 poorly labeled cells, presumably due to competing precipitation when water solubility drops below 20 pM (Figure 4a). The flippers that reached the plasma membrane were rapidly internalized and labeled less ordered intracellular membranes at shorter lifetimes (Figure 7).

Increasing internalization with increasing LogP of the flipper probe might appear counterintuitive. It could suggest that without intermembrane transfer, the permanent presence in the plasma membrane increases endocytosis. Alternatively, increasing stability of non-emissive micelles with decreasing monomer solubility could hinder their fluorogenic disassembly upon arrival to the plasma membrane, which could result in uptake of the entire nanoparticle and fluorogenic disassembly only within the cell.

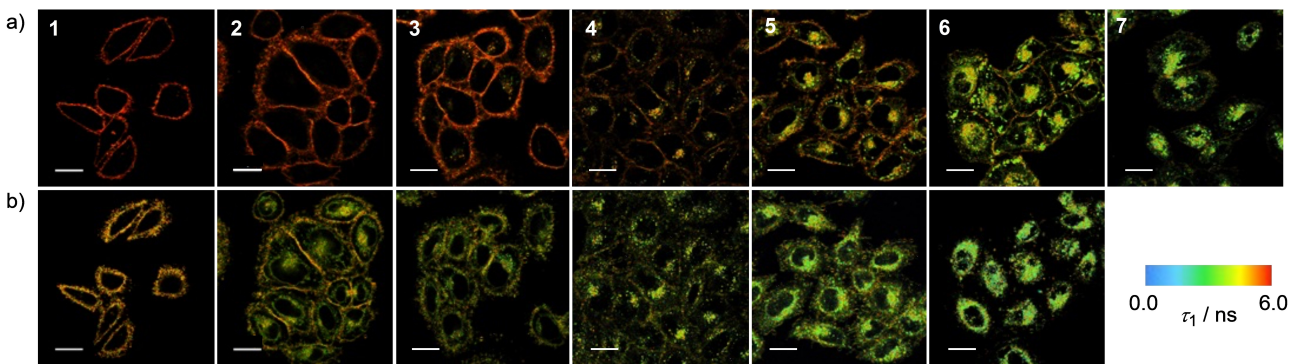


Figure 7. FLIM images of flipper probes 1–7 added to HK cells (a) before and (b) after hyperosmotic shock. Scale bars = 20  $\mu$ m.

FLIM lifetimes of H-Flipper **2** and G-Flipper **3** in plasma membrane of HK cells were 5.1 and 5.2 ns, 0.4 to 0.3 ns shorter than 5.5 ns of the original **1** (Table 1). This decrease was consistent with the lifetimes  $\tau_{o+d}$  in GUVs, which also decreased slightly for **2** and **3** (Figure 5e). Moreover, the shorter lifetimes of **2** and **3** compared to **1** in plasma membranes were consistent with increasing  $L_d$  labeling in multi-component GUVs, which corresponds to an increasing population of twisted flippers with shorter lifetime.

After the osmotic shock, lifetimes counted in the plasma membrane only decreased for both H-Flipper **2** and G-Flipper **3** to 4.5 ns (Table 1). In comparison, lifetimes of Flipper-TR® **1** decreased from 5.5 ns to 5.0 ns (Table 1). The lifetime changes in response to membrane tension thus increased from **1** to **2** and **3**. This was of interest because lifetime changes determine the responsiveness of fluorescent membrane tension probes. To increase the lifetime of fluorescent membrane tension probes, that is their sensitivity or brightness, increasing partitioning into  $L_o$  domains by hydrophobic interfacing is most important. To increase the responsiveness of membrane tension probes, however, increasing partitioning into  $L_d$ , rather than  $L_o$  membranes, might thus deserve attention as well.

## Conclusions

The objective of this study was to explore the importance of hydrophobic interfacing of fluorescent membrane probes for bioimaging. Flipper probes were ideal for this purpose because of their sensitive response to different environments. The collection of interfacers assessed with flippers **2**–**7** provided complex but consistent insights that will be helpful for future probe design.

The main findings are, first, that intermembrane transfer can be suppressed by finetuning the hydrophobic interfacing, thus answering an important question with regard to intracellular targeting. However, less water soluble amphiphiles are also rapidly internalized, either as membrane-bound monomers by endocytosis or as non-emissive micelles that disassemble only within the cells. Second, inversion of the selectivity of interdomain transfer from  $L_d$  to  $L_o$  domains is possible by hydrophobic interfacing, a finding that allows to improve on

sensitivity and responsiveness of membrane tension imaging in living cells. Third, evidence for the occurrence of two-step insertion to  $L_o$  domains through  $L_d$  domains followed by intramembrane transfer is secured and explains differences between partition coefficients from single-component model membranes and results from multi-component GUVs as well as bioimaging. Fourth, hydrophobic matching is shown to improve spectral signatures and subphase recognition in ordered membranes. The conclusion that matching shape of the interfacers is more important than matching length is consistently supported throughout the study. These results are important because they demonstrate that hydrophobic interfacing can improve the performance of membrane probes.

For practical probe design, our results suggest that the labeling of  $L_d$  and  $L_o$  domains in GUVs correlates well with cellular performance. High  $L_o$  labeling affords long lifetimes, that is sensitivity or brightness, while high  $L_d$  labeling might afford large lifetime differences, that is responsiveness to changes in membrane tension. The labeling of  $L_d$  and  $L_o$  domains in GUVs is not predicted by partition coefficients because two-step partitioning and differences in fluorescence intensity are ignored. However, the labeling of  $L_d$  and  $L_o$  domains in multi-component GUVs correlates well with red shifts with increasing  $L_o$  content in multi-component  $L_o+L_d$  LUVs and the finestructure of deconvoluted excitation spectra in single-component  $S_o$  LUVs. This finestructure can be quantified by a positioning factor that can be predictive for hydrophobic interfacing and  $L_o$  labeling.

The possible impact of increasing labeling of  $L_o$  domains and improved hydrophobic interfacing of flippers **4**–**6** on membrane tension imaging in plasma membranes of living cells could not be assessed because of rapid internalization by monomer endocytosis or as micellar nanoparticles. One possibility to solve this dilemma would be to tether the probes to an existing membrane protein or a specifically engineered protein like the Halo Tag. Although the feasibility of this solution has been validated previously with HaloFlippers, it requires genetic engineering and limits imaging to local protein environments.<sup>[56,63]</sup> For practical and general use in the community, small-molecule probes that just can be added to the cells would be preferable. Lessons learned in this study demonstrate that hydrophobic interfacing in the plasma



membrane should be possible if the impact on intermembrane transfer is compensated by complementary headgroup engineering. Because of the significance of flipper probes and the here reported evidence that hydrophobic interfacing can improve performance, studies along this line are justified despite the synthetic effort involved. In general, our results show that hydrophobic interfacing matters for probe performance and give directions on how to proceed with a complex system that is hyperresponsive to multiple parameters. The practical usefulness of these lessons learned to design better fluorescent membrane tension probes is currently being explored.

## Experimental Section

Please see Supporting Information.<sup>[57,59,69,76,81–85]</sup>

## Acknowledgements

We thank the NMR, MS, ACCESS and Bioimaging platforms for services, and the University of Geneva, the National Centre of Competence in Research (NCCR) Chemical Biology (51NF40-185898), the NCCR Molecular Systems Engineering (51NF40-205608), as well as the Swiss NSF for financial support (Excellence Grant 200020 204175; Swiss-ERC Advanced Grant TIMEUP, TMAG-2\_209190).

## Conflict of Interests

The University of Geneva has licensed Flipper-TR® probes to Spirochrome for commercialization.

## Data Availability Statement

The data that support the findings of this study are openly available at <https://doi.org/10.5281/zenodo.8256213>.

**Keywords:** bioimaging · fluorescent probes · giant unilamellar vesicles · hydrophobic matching · intermembrane transfer · mechanosensitive probes · membrane domains · membrane probes · partitioning

- [1] A. S. Klymchenko, *Acc. Chem. Res.* **2017**, *50*, 366–375.
- [2] T. Baumgart, G. Hunt, E. R. Farkas, W. W. Webb, G. W. Feigenson, *Biochim. Biophys. Acta* **2007**, *1768*, 2182–2194.
- [3] E. Sezgin, T. Sadowski, K. Simons, *Langmuir* **2014**, *30*, 8160–8166.
- [4] P. Liu, E. W. Miller, *Acc. Chem. Res.* **2020**, *53*, 11–19.
- [5] X.-X. Chen, F. Bayard, N. Gonzalez-Sanchis, K. K. P. Pamungkas, N. Sakai, S. Matile, *Angew. Chem. Int. Ed.* **2023**, *62*, e202217868.
- [6] M. Páez-Pérez, I. López-Duarte, A. Vyšniauskas, N. J. Brooks, M. K. Kuimova, *Chem. Sci.* **2020**, *12*, 2604–2613.
- [7] P.-Y. Ho, T. Y. Chou, C. Kam, W. Huang, Z. He, A. H. W. Ngan, S. Chen, *Sci. Adv.* **2023**, *9*, eabn5390.
- [8] Y. Zhao, H. S. Kim, X. Zou, L. Huang, X. Liang, Z. Li, J. S. Kim, W. Lin, *J. Am. Chem. Soc.* **2022**, *144*, 20854–20865.

- [9] A. Vyšniauskas, M. Balaz, H. L. Anderson, M. K. Kuimova, *Phys. Chem. Chem. Phys.* **2015**, *17*, 7548–7554.
- [10] I. López-Duarte, T. T. Vu, M. A. Izquierdo, J. A. Bull, M. K. Kuimova, *Chem. Commun.* **2014**, *50*, 5282–5284.
- [11] X. Peng, Z. Yang, J. Wang, J. Fan, Y. He, F. Song, B. Wang, S. Sun, J. Qu, J. Qi, M. Yan, *J. Am. Chem. Soc.* **2011**, *133*, 6626–6635.
- [12] L. Wang, Y. Xiao, W. Tian, L. Deng, *J. Am. Chem. Soc.* **2013**, *135*, 2903–2906.
- [13] Z. Yang, Y. He, J.-H. Lee, N. Park, M. Suh, W.-S. Chae, J. Cao, X. Peng, H. Jung, C. Kang, J. S. Kim, *J. Am. Chem. Soc.* **2013**, *135*, 9181–9185.
- [14] Z. Yang, D. H. Kang, H. Lee, J. Shin, W. Yan, B. Rathore, H.-R. Kim, S. J. Kim, H. Singh, L. Liu, J. Qu, C. Kang, J. S. Kim, *Bioconjugate Chem.* **2018**, *29*, 1446–1453.
- [15] I. E. Steinmark, A. L. James, P.-H. Chung, P. E. Morton, M. Parsons, C. A. Dreiss, C. D. Lorenz, G. Yahiroglu, K. Suhling, *PLoS One* **2019**, *14*, e0211165.
- [16] X. Li, M. Tian, G. Zhang, R. Zhang, R. Feng, L. Guo, X. Yu, N. Zhao, X. He, *Anal. Chem.* **2017**, *89*, 3335–3344.
- [17] X. Li, R. Zhang, L. Guo, H. Zhang, F. Meng, R. Yang, C. Li, Z. Liu, X. Yu, *Anal. Chem.* **2019**, *91*, 2672–2677.
- [18] J. Hong, X. Guan, Y. Chen, X. Tan, S. Zhang, G. Feng, *Anal. Chem.* **2023**, *95*, 5687–5694.
- [19] R. Kimura, H. Kuramochi, P. Liu, T. Yamakado, A. Osuka, T. Tahara, S. Saito, *Angew. Chem. Int. Ed.* **2020**, *59*, 16430–16435.
- [20] Z. Zhang, G. Sun, W. Chen, J. Su, H. Tian, *Chem. Sci.* **2020**, *11*, 7525–7537.
- [21] C.-H. Wu, Y. Chen, K. A. Pyrshev, Y.-T. Chen, Z. Zhang, K.-H. Chang, S. O. Yesylevskyy, A. P. Demchenko, P.-T. Chou, *ACS Chem. Biol.* **2020**, *15*, 1862–1873.
- [22] N. P. Kamat, Z. Liao, L. E. Moses, J. Rawson, M. J. Therien, I. J. Dmochowski, D. A. Hammer, *Proc. Natl. Acad. Sci. USA* **2011**, *108*, 13984–13989.
- [23] S. Sasaki, S. Suzuki, W. M. C. Sameera, K. Igawa, K. Morokuma, G. Konishi, *J. Am. Chem. Soc.* **2016**, *138*, 8194–8206.
- [24] H. V. Humeniuk, A. Rosspeintner, G. Licari, V. Kilin, L. Bonacina, E. Vauthay, N. Sakai, S. Matile, *Angew. Chem. Int. Ed.* **2018**, *57*, 10559–10563.
- [25] G. Singh, G. George, S. O. Raja, P. Kandaswamy, M. Kumar, S. Thutupalli, S. Laxman, A. Gulyani, *Proc. Natl. Acad. Sci. USA* **2023**, *120*, e2213241120.
- [26] Y. Zheng, Y. Ding, J. Ren, Y. Xiang, Z. Shuai, A. Tong, *Anal. Chem.* **2020**, *92*, 14494–14500.
- [27] J. M. Kwiatak, D. M. Owen, A. Abu-Siniyeh, P. Yan, L. M. Loew, K. Gaus, *PLoS One* **2013**, *8*, e52960.
- [28] D. I. Danylchuk, P.-H. Jouard, A. S. Klymchenko, *J. Am. Chem. Soc.* **2021**, *143*, 912–924.
- [29] L. Jin, A. C. Millard, J. P. Wuskell, X. Dong, D. Wu, H. A. Clark, L. M. Loew, *Biophys. J.* **2006**, *90*, 2563–2575.
- [30] D. M. Owen, P. M. P. Lanigan, C. Dunsby, I. Munro, D. Grant, M. A. A. Neil, P. M. W. French, A. I. Magee, *Biophys. J.* **2006**, *90*, L80–82.
- [31] N. Sakai, S. Matile, *J. Am. Chem. Soc.* **2018**, *140*, 11438–11443.
- [32] Y. Bagheri, A. A. Ali, P. Keshri, J. Chambers, A. Gershenson, M. You, *Angew. Chem. Int. Ed.* **2022**, *61*, e202112033.
- [33] A. S. Klymchenko, S. Oncul, P. Didier, E. Schaub, L. Bagatolli, G. Duportail, Y. Mély, *Biochim. Biophys. Acta* **2009**, *1788*, 495–499.
- [34] N. Li, W. Zhang, H. Lin, J.-M. Lin, *Chin. Chem. Lett.* **2022**, *33*, 1377–1380.
- [35] M. Tasior, O. Vakuliuk, D. Koga, B. Koszarna, K. Górska, M. Grzybowski, Ł. Kieleski, M. Krzeszewski, D. T. Gryko, *J. Org. Chem.* **2020**, *85*, 13529–13543.
- [36] D. Thomas, V. Rubio, V. Iragavarapu, E. Guzman, O. B. Pelletier, S. Alamgir, Q. Zhang, M. J. Stawikowski, *ACS Chem. Neurosci.* **2021**, *12*, 719–734.
- [37] E. Sezgin, F. Schneider, V. Zilles, I. Urbančič, E. Garcia, D. Waithe, A. S. Klymchenko, C. Eggeling, *Biophys. J.* **2017**, *113*, 1321–1330.
- [38] J. H. Lorent, K. R. Levental, L. Ganesan, G. Rivera-Longsworth, E. Sezgin, M. Doktorova, E. Lyman, I. Levental, *Nat. Chem. Biol.* **2020**, *16*, 644–652.
- [39] G. Duportail, A. Klymchenko, Y. Mely, A. Demchenko, *FEBS Lett.* **2001**, *508*, 196–200.
- [40] Z. Turkmen, A. S. Klymchenko, S. Oncul, G. Duportail, G. Topcu, A. P. Demchenko, *J. Biochem. Biophys. Methods* **2005**, *64*, 1–18.
- [41] R. Prasad, A. Sliwa-Gonzalez, Y. Barral, *Sci. Adv.* **2020**, *6*, eaba5130.
- [42] S. Rodriguez-Gallardo, K. Kurokawa, S. Sabido-Bozo, A. Cortes-Gomez, A. Ikeda, V. Zoni, A. Aguilera-Romero, A. M. Perez-Linero, S. Lopez, M. Waga, M. Araki, M. Nakano, H. Riezman, K. Funato, S. Vanni, A. Nakano, M. Muñiz, *Sci. Adv.* **2020**, *6*, eaba8237.
- [43] T. Chen, A. Ghosh, J. Enderlein, *Nano Lett.* **2023**, *23*, 2421–2426.



- [44] B. Ghebremariam, V. Sidorov, S. Matile, *Tetrahedron Lett.* **1999**, *40*, 1445–1448.
- [45] P. Yan, A. Xie, M. Wei, L. M. Loew, *J. Org. Chem.* **2008**, *73*, 6587–94.
- [46] J. E. Reeve, A. D. Corbett, I. Boczarow, W. Kaluza, W. Barford, H. Bayley, T. Wilson, H. L. Anderson, *Angew. Chem. Int. Ed.* **2013**, *52*, 9044–9048.
- [47] O. Murata, Y. Shindo, Y. Ikeda, N. Iwasawa, D. Citterio, K. Oka, Y. Hiruta, *Anal. Chem.* **2020**, *92*, 966–974.
- [48] A. Podder, M. M. Joseph, S. Biswas, S. Samanta, K. K. Maiti, S. Bhuniya, *Chem. Commun.* **2021**, *57*, 607–610.
- [49] C. Wang, M. Taki, K. Kajiwara, J. Wang, S. Yamaguchi, *ACS Materials Lett.* **2020**, *2*, 705–711.
- [50] L. Assies, V. Mercier, J. López-Andarias, A. Roux, N. Sakai, S. Matile, *ChemBioChem* **2022**, *23*, e202200192.
- [51] A. Fin, A. Vargas Jentsch, N. Sakai, S. Matile, *Angew. Chem. Int. Ed.* **2012**, *51*, 12736–12739.
- [52] B. Baumeister, S. Matile, *Chem. Eur. J.* **2000**, *6*, 1739–1749.
- [53] K. Sato, T. Muraoka, K. Kinbara, *Acc. Chem. Res.* **2021**, *54*, 3700–3709.
- [54] N. Sakai, L. Assies, S. Matile, *Helv. Chim. Acta* **2022**, *105*, e202200052.
- [55] F. Piazzolla, V. Mercier, L. Assies, N. Sakai, A. Roux, S. Matile, *Angew. Chem. Int. Ed.* **2021**, *60*, 12258–12263.
- [56] K. Straková, J. López-Andarias, N. Jiménez-Rojo, J. E. Chambers, S. J. Marciak, H. Riezman, N. Sakai, S. Matile, *ACS Cent. Sci.* **2020**, *6*, 1376–1385.
- [57] J. García-Calvo, J. López-Andarias, N. Sakai, S. Matile, *Helv. Chim. Acta* **2022**, *105*, e202100238.
- [58] J. García-Calvo, J. López-Andarias, J. Maillard, V. Mercier, C. Roffay, A. Roux, A. Fürstenberg, N. Sakai, S. Matile, *Chem. Sci.* **2022**, *13*, 2086–2093.
- [59] K. Strakova, A. I. Poblador-Bahamonde, N. Sakai, S. Matile, *Chem. Eur. J.* **2019**, *25*, 14935–14942.
- [60] G. Licari, K. Strakova, S. Matile, E. Tajkhorshid, *Chem. Sci.* **2020**, *11*, 5637–5649.
- [61] F. Neuhaus, F. Zobi, G. Brezesinski, M. Dal Molin, S. Matile, A. Zumbuehl, *Beilstein J. Org. Chem.* **2017**, *13*, 1099–1105.
- [62] J. López-Andarias, K. Straková, R. Martinent, N. Jiménez-Rojo, H. Riezman, N. Sakai, S. Matile, *JACS Au* **2021**, *1*, 221–232.
- [63] J. López-Andarias, K. Eblihatian, Q. T. L. Pasquer, L. Assies, N. Sakai, S. Hoogendoorn, S. Matile, *Angew. Chem. Int. Ed.* **2022**, *61*, e202113163.
- [64] P. Müller, J. Nikolaus, S. Schiller, A. Herrmann, K. Möllnitz, S. Czapla, P. Wessig, *Angew. Chem. Int. Ed.* **2009**, *48*, 4433–4435.
- [65] M. R. R. de Planque, J. A. Killian, *Mol. Membr. Biol.* **2003**, *20*, 271–284.
- [66] J. A. Killian, G. von Heijne, *Trends Biochem. Sci.* **2000**, *25*, 429–434.
- [67] M. Macchione, M. Tsemperouli, A. Goujon, A. R. Mallia, N. Sakai, K. Sugihara, S. Matile, *Helv. Chim. Acta* **2018**, *101*, e1800014.
- [68] X.-X. Chen, R. M. Gomila, J. M. García-Arcos, M. Vonesch, N. Gonzalez-Sanchis, A. Roux, A. Frontera, N. Sakai, S. Matile, *JACS Au* **2023**, *3*, 2557–2565.
- [69] S. Soleimanpour, A. Colom, E. Derivery, M. Gonzalez-Gaitan, A. Roux, N. Sakai, S. Matile, *Chem. Commun.* **2016**, *52*, 14450–14453.
- [70] M. Macchione, N. Chuard, N. Sakai, S. Matile, *ChemPlusChem* **2017**, *82*, 1062–1066.
- [71] R. Koynova, M. Caffrey, *Biochim. Biophys. Acta* **1998**, *1376*, 91–145.
- [72] C. M. González-Henríquez, V. A. Villegas-Opazo, D. H. Sagredo-Oyarce, M. A. Sarabia-Vallejos, C. A. Terraza, *Biосensors* **2017**, *7*, 34.
- [73] K. Akabori, J. F. Nagle, *Soft Matter* **2015**, *11*, 918–926.
- [74] C. Zhong, *Phys. Chem. Chem. Phys.* **2015**, *17*, 9248–9257.
- [75] Q. Verolet, A. Rosspeintner, S. Soleimanpour, N. Sakai, E. Vauthey, S. Matile, *J. Am. Chem. Soc.* **2015**, *137*, 15644–15647.
- [76] J. García-Calvo, J. Maillard, I. Furera, K. Strakova, A. Colom, V. Mercier, A. Roux, E. Vauthey, N. Sakai, A. Fürstenberg, S. Matile, *J. Am. Chem. Soc.* **2020**, *142*, 12034–12038.
- [77] A. Daina, O. Michielin, V. Zoete, *Sci. Rep.* **2017**, *7*, 42717.
- [78] S. H. White, W. C. Wimley, A. S. Ladokhin, K. Hristova, *Methods Enzymol.* **1998**, *295*, 62–87.
- [79] T. M. Konyakhina, J. Wu, J. D. Mastrianni, F. A. Heberle, G. W. Feigenson, *Biochim. Biophys. Acta* **2013**, *1828*, 2204–2214.
- [80] R. S. Petruzielo, F. A. Heberle, P. Drazba, J. Katsaras, G. W. Feigenson, *Biochim. Biophys. Acta* **2013**, *1828*, 1302–1313.
- [81] Q. Laurent, N. Sakai, S. Matile, *Chem. Eur. J.* **2022**, *28*, e202200785.
- [82] K. Suthagar, A. J. Fairbanks, *Chem. Commun.* **2017**, *53*, 713–715.
- [83] J. De Vrieze, A. P. Baptista, L. Nuhn, S. Van Herck, K. Deswarte, H. Yu, B. N. Lambrecht, B. G. De Geest, *Adv. Ther.* **2021**, *4*, 2100079.
- [84] E. D. Goddard-Borger, R. V. Stick, *Org. Lett.* **2007**, *9*, 3797–3800.
- [85] J. Bachl, J. Mayr, F. J. Sayago, C. Cativiela, D. D. Díaz, *Chem. Commun.* **2015**, *51*, 5294–5297.

Version of record online: October 2, 2023